Theory for the nonlinear magneto-optical Kerr effect at ferromagnetic transition-metal surfaces

U. Pustogowa, W. Hübner, and K. H. Bennemann
Institute for Theoretical Physics, Freie Universität Berlin, Arnimallee 14, 1000 Berlin 33, Germany
(Received 2 February 1993; revised manuscript received 19 May 1993)

We present a theory for the nonlinear magneto-optical Kerr spectrum of Fe by extending our previous analysis. The obtained results are compared with recent experimental data for a Fe(110) surface. The various general features of the nonlinear Kerr effect, the detailed dependence of the Kerr spectrum on exchange interaction, and Fermi-level crossing on frequency and spin-orbit interaction are discussed. In particular, we demonstrate how the spectrum depends on *d*-band width and *sd* hybridization. Thus, we are able to extract band narrowing due to electronic correlations or due to a reduced coordination number from the spectra. The latter is particularly relevant for thin films. To shed further light on the dependence of the nonlinear Kerr spectrum on electronic parameters we also calculate the linear magneto-optical Kerr effect. The differences between the Kerr spectra of Fe and Ni are discussed.

I. INTRODUCTION

The nonlinear magneto-optical Kerr effect (NLMOKE) describes the rotation of the polarization plane for second-harmonic generation (SHG) in reflection from a ferromagnetic sample surface. This effect reflects the symmetry of the surface structure and surface magnetism and has been proposed as an ultrafast spectroscopic probe for the investigation of two-dimensional (2D) magnetism.[1–3] The NLMOKE is very well suited for a direct investigation of surface structures and electronic and magnetic properties. Thus, two-dimensional ferromagnetic structures at surfaces, interfaces, in thin magnetic films, and multilayers can be studied. In combination with optical "pump and probe" techniques the nonlinear magneto-optical Kerr effect allows a time-dependent study of 2D magnetism on the picosecond through femtosecond time scale. Since it seems conceivable to apply the NLMOKE for layer-by-layer magneto-optical recording this effect is interesting for the development of magneto-optical storage media. Note that in contrast to nonoptical studies the nonlinear Kerr effect is destructionless and not restricted to the study of remanent magnetization. As the NLMOKE is caused by the interplay of spin-orbit coupling and exchange interaction it becomes important for the determination of the spin-orbit interaction-induced magnetocrystalline anisotropy. Furthermore, the nonlinear magneto-optical Kerr effect can be used for measuring the spin-lattice relaxation time.[4] Note, the spin-lattice relaxation time is the ultimate time and speed limit for magneto-optical recording technologies. This relaxation time contains spin-orbit coupling via phonon-magnon interaction (in transition metals).

The first microscopic calculations of NLMOKE spectra have been performed for a nickel surface.[1,2] The nonlinear magneto-optical tensor has been derived using an equation-of-motion method for the density operator. The band structure needed as an input has been treated as a superposition of Brillouin spheres. In a subsequent work, the calculation has been extended[5] to a fully three-dimensional anisotropic band structure. Also the linear and nonlinear Kerr spectra of Ni have been calculated taking into account the complete **k**-dependent dipole transition-matrix elements. The resulting spectra were compared with those obtained by using constant matrix elements. The basic conclusions of this previous work have been the following. (i) The nonlinear magneto-optical Kerr effect should be detectable in experiment and should be sensitive to 2D magnetism. (ii) The peak positions and peak-height ratios of the MOKE and NLMOKE spectra are determined by the electronic band structure. (iii) The influence of the matrix elements is only moderate and affects mainly the absolute magnitude of the spectra and the peak widths.

Motivated by these theoretical studies first experiments on Fe were performed in 1991 (Reif *et al.*[6]). The (110) surface of single-crystal Fe in a single-domain state was studied under ultrahigh-vacuum conditions. Upon reversing the direction of the in-plane magnetization with the help of a weak external magnetic field defining the quantization axis a drastic change of the SHG yield was observed. For the clean Fe (110) surface the ratio of the nonlinear magnetic-to-nonmagnetic susceptibility amounts to 25%. This value is in agreement with the theoretical prediction which is 27%. Note, the theoretical ratio was obtained by scaling the theory for Ni by the ratio of the bulk magnetic moments of Fe and Ni. The validity of such a scaling law is discussed in detail in Sec. IV. Clearly it is necessary to check this crude approximation by a microscopic calculation as will be done in this study.

If the Fe surface is deliberately contaminated by chemisorbing CO an exponential decay of the *magnetic* signal is observed, whereas the *nonmagnetic* contribution to the signal remains constant. This dramatic influence of contamination clearly demonstrates the sensitivity of this technique for surface *magnetism*. Further observations show that the SHG signal vanishes if the surface is

intentionally damaged by a too strong laser pulse.

Besides comparing with the experimental results by Reif *et al.*, it is of general interest to analyze theoretically the differences between the Kerr-effect spectra of iron and nickel. The differences regarding the magnetic properties, such as the exchange splitting and magnetic moments and also the crystal structure, require an extension of our previous theory. For Fe one expects a reduction of electronic many-body effects and at the same time an increase of geometric structure effects. The surfaces of Fe are not as smooth as those of Ni where many-body effects play a dominant role.[7,8] Thus, a larger wave-function basis set for the electronic band-structure calculation is necessary. In addition, we should treat in a better way the boundary points in the irreducible portion ($\frac{1}{48}$) of the bcc Brillouin zone. Furthermore, by varying different values of the band structure (d-band width, s-band position, exchange splitting), we expect a more-detailed understanding of the parameters controlling the features of the spectrum. This will be also useful for a systematic understanding of the nonlinear Kerr effect in different ferromagnetic transition metals and for an extension of our theory to interfaces, thin magnetic films, and magnetic alloys.

One expects that the comparison of the linear and nonlinear Kerr spectra will help to shed light on the essential material parameters responsible for the shape of the spectra. Therefore, we also calculate the corresponding linear magneto-optical Kerr spectra and compare with experiments[9–11] and different linear MOKE calculations.[12–15]

In Sec. II we briefly present the previously developed theory and its extension to iron. In Sec. III we show our results for the nonlinear Kerr spectra of Fe. In Sec. IV, general features of the Kerr spectrum are analyzed and we explain the experimental results for Fe (Ref. 6) using our theory. In Appendix A we show that our linear-response function can be related to the corresponding expression given by Wang and Callaway.[16]

II. THEORY

The linear and nonlinear magneto-optical Kerr effects result from the combined action of exchange interaction and spin-orbit coupling. Spin-orbit coupling acts on the electrons like an external magnetic field and thus rotates the polarization plane of the reflected light. The Kerr spectra are given by the susceptibilities which are determined using response theory,

$$\mathbf{P}(\mathbf{q},\omega) = \chi^{(1)}(\mathbf{q},\omega,\mathbf{M})\mathbf{E}(\mathbf{q},\omega) + \chi^{(2)}(2\mathbf{q},2\omega,\mathbf{M})\mathbf{E}(\mathbf{q},\omega)\mathbf{E}(\mathbf{q},\omega) + \cdots , \tag{1}$$

where $\mathbf{P}(\mathbf{q},\omega)$ is the polarization of wave vector $\mathbf{q}$ and frequency ω caused by the total electric field $\mathbf{E}(\mathbf{q},\omega)$, due to the incident light. In the following paragraph the linear susceptibility $\chi^{(1)}(\mathbf{q},\omega,\mathbf{M})$ is presented for the case of polar geometry, where $\mathbf{M}$ is directed vertical to the surface along the z axis, and the nonlinear susceptibility $\chi^{(2)}(2\mathbf{q},2\omega,\mathbf{M})$ for the case of in-plane magnetization ($\mathbf{M}$ parallel to the y axis). First one finds, following the self-consistent-field approach by Ehrenreich and Cohen[17] for the linear response, the expression

$$\chi^{(1)}_{xy}(\mathbf{q},\omega,\mathbf{M}) = \frac{e^2}{\Omega}\frac{\lambda_{\text{s.o.}}}{\hbar\omega}\sum_{\mathbf{k},l,l',\sigma}\left[\langle\mathbf{k}+\mathbf{q},l'\sigma|y|\mathbf{k}l\sigma\rangle\langle\mathbf{k}l\sigma|x|\mathbf{k}+\mathbf{q},l'\sigma\rangle\frac{f(E_{\mathbf{k}+\mathbf{q},l'\sigma})-f(E_{\mathbf{k}l\sigma})}{E_{\mathbf{k}+\mathbf{q},l'\sigma}-E_{\mathbf{k}l\sigma}-\hbar\omega+i\hbar\alpha_1}\right]. \tag{2}$$

Here magnetism is included by the spin dependence (σ) of the electronic energies $E_{\mathbf{k}l\sigma}$, $E_{\mathbf{k}+\mathbf{q},l'\sigma}$ and the wave functions $|\mathbf{k}l\sigma\rangle$, $|\mathbf{k}+\mathbf{q},l'\sigma\rangle$. In Eq. (2) the following symbols are used: $\lambda_{\text{s.o.}}$ is the spin-orbit coupling constant, $|\mathbf{k}l\sigma\rangle = \frac{1}{\sqrt{\Omega}}u_{\mathbf{k}l\sigma}e^{i\mathbf{k}\cdot\mathbf{r}}$ are Bloch states of wave vector $\mathbf{k}$ and spin σ in the lth band, $E_{\mathbf{k}l\sigma}$ is the band structure of the irradiated material, and α_1 is the experimental resolution. Ω refers to the volume. Effects due to spin-orbit coupling are included in the wave functions by using linear perturbation theory. Note that spin-orbit coupling effects the electronic energies much less. It is interesting that Eq. (2) contains the corresponding expression given previously by Wang and Callaway,[16] see the discussion in Appendix A. Equation (2) includes the plasma resonance in the limit $q \longrightarrow 0$, $l = l'$ (intraband transitions), see Ref. 18 and Appendix A. Second, the nonlinear response function can also be obtained by extending the procedure by Ehrenreich and Cohen and is given by

$$\chi^{(2)}_{xzz}(2\mathbf{q}_\parallel,2\omega,\mathbf{M}) = \frac{e^3\mathbf{q}_\parallel a}{\Omega}\frac{\lambda_{\text{s.o.}}}{\hbar\omega}\sum_{\sigma}\sum_{\mathbf{k},l,l',l''}\langle\mathbf{k}+2\mathbf{q}_\parallel,l''\sigma|x|\mathbf{k}l\sigma\rangle\langle\mathbf{k}l\sigma|z|\mathbf{k}+\mathbf{q}_\parallel,l'\sigma\rangle\langle\mathbf{k}+\mathbf{q}_\parallel,l'\sigma|z|\mathbf{k}+2\mathbf{q}_\parallel,l''\sigma\rangle \times\frac{\frac{f(E_{\mathbf{k}+2\mathbf{q}_\parallel,l''\sigma})-f(E_{\mathbf{k}+\mathbf{q}_\parallel,l'\sigma})}{E_{\mathbf{k}+2\mathbf{q}_\parallel,l''\sigma}-E_{\mathbf{k}+\mathbf{q}_\parallel,l'\sigma}-\hbar\omega+i\hbar\alpha_1}-\frac{f(E_{\mathbf{k}+\mathbf{q}_\parallel,l'\sigma})-f(E_{\mathbf{k}l\sigma})}{E_{\mathbf{k}+\mathbf{q}_\parallel,l'\sigma}-E_{\mathbf{k}l\sigma}-\hbar\omega+i\hbar\alpha_1}}{E_{\mathbf{k}+2\mathbf{q}_\parallel,l''\sigma}-E_{\mathbf{k}l\sigma}-2\hbar\omega+i2\hbar\alpha_1}. \tag{3}$$

Here, the photon wave vector parallel to the surface is denoted by $\mathbf{q}_\parallel$ and a is the lattice constant. For a detailed derivation of Eqs. (2) and (3) see Refs. 2 and 5 and Appendix A. Furthermore, note that a linear correction of only one of the wave functions due to spin-orbit coupling has been taken into account. This seems justified in view of the observation by Misemer[12] that the results obtained either by diagonalizing the Hamilton operator

including $\lambda_{s.o.}$ or applying first-order perturbation theory to the wave functions are identical. The factor $\frac{\lambda_{s.o.}}{\hbar\omega}$ in Eqs. (2) and (3) results from replacing $\langle \mathbf{k}l\sigma|$ by $\frac{\lambda_{s.o.}}{\hbar\omega}\langle \mathbf{k}l\sigma|$, which can at least be justified for the optical part of the spectrum; see also Appendix A. Regarding many-body effects, vertex corrections have been neglected in Eqs. (2) and (3), while self-energy corrections are still included.

The complex angle ϕ_K of the linear Kerr effect in the *polar* geometry (incident beam, reflected beam, and magnetization perpendicular to the surface) is given by the diagonal and off-diagonal elements of the magneto-optical susceptibility tensor

$$\phi_K \equiv \varphi_K + i\varepsilon_K = -\frac{\chi^{(1)}_{xy}}{\chi^{(1)}_{xx}\sqrt{1+4\pi\chi^{(1)}_{xx}}}. \tag{4}$$

Here, φ_K is the actually measured Kerr angle and ε_K is the ellipticity of the reflected-light polarization. The tensors $\chi^{(1)}_{xy}(\mathbf{q},\omega,\mathbf{M})$ and $\chi^{(2)}_{xzz}(2\mathbf{q}_\parallel, 2\omega, \mathbf{M})$ are tensors of rank two and three, respectively. In centrosymmetric media, $\chi^{(2)}_{xzz}(2\mathbf{q}_\parallel, 2\omega, \mathbf{M})$ vanishes exactly due to the product of three parity-changing dipole matrix elements, except for the surface (or buried interface) where the crystal symmetry is broken. The photons of frequency ω induce oscillating dipole moments leading to a surface charge of frequency ω which in turn interacts with the incoming photons and becomes the source of the frequency-doubled reflected light. This holds also in the presence of a finite magnetization $\mathbf{M}$. Thus, the NLMOKE tensor $\chi^{(2)}_{xzz}(2\mathbf{q}_\parallel, 2\omega, \mathbf{M})$ probes the geometric, electronic, and magnetic properties of the surface layer. It contains the electronic surface properties explicitly in the band structure $E_{\mathbf{k}l\sigma}$, the geometrical arrangement of the atoms in the k-space anisotropy of the band structure, and the ferromagnetism in the spin indices of the wave functions and the exchange-split energy bands. The linear and nonlinear Kerr effects result from the action of the spin-orbit coupling on the wave functions which allows for nonvanishing off-diagonal elements of the linear and nonlinear magneto-optical tensors, thus leading to finite Kerr angles in exchange-split bands. Clockwise and counterclockwise rotations of the polarization plane caused by electrons with majority and minority spin, respectively, no longer cancel in ferromagnets as they do in paramagnets, since the densities of states for majority and minority electrons are different.

The quantities required for the microscopic calculation of the nonlinear magneto-optical Kerr susceptibility $\chi^{(2)}_{xzz}(2\mathbf{q}_\parallel, 2\omega, \mathbf{M})$ in Eq. (3) are the exchange-split band structure $E_{\mathbf{k}l\sigma}$ and the dipole matrix elements. To determine the states, energies, and matrix elements, the band structure of bulk iron is calculated employing the semiempirical combined interpolation scheme proposed by Hodges, Ehrenreich, and Lang.[19] The method has also been used by Baker and Smith[20] for paramagnetic iron and by Misemer.[12] This method employs a useful parametrized band structure.

Hence we calculate the iron band structure using pseudopotentials for the *sp* part and the tight-binding technique for the *d* orbitals. For these we use a basis set of 12 wave functions per spin. Seven of these wave functions are plane waves to account for the $4s$ orbitals $\Phi_i(\mathbf{k},\mathbf{r}) = e^{i(\mathbf{k}+\mathbf{K}_i)\cdot\mathbf{r}}$ $(i = 1,\ldots,7)$, and five linear combinations of atomic orbitals describe the $3d$ electrons: $\psi_\mu(\mathbf{k},\mathbf{r}) = \frac{1}{\sqrt{N}}\sum_l e^{i\mathbf{k}\cdot\mathbf{R}_l}\varphi_\mu(\mathbf{r}-\mathbf{R}_l)$ $(\mu = 8,\ldots,12)$. Here $\varphi_\mu(\mathbf{r}-\mathbf{R}_l)$ are atomic d orbitals centered at site $\mathbf{R}_l$: $\varphi_1(\mathbf{r}) = \frac{xy}{r^2}f(r)$, $\varphi_2(\mathbf{r}) = \frac{yz}{r^2}f(r)$, $\varphi_3(\mathbf{r}) = \frac{xz}{r^2}f(r)$, $\varphi_4(\mathbf{r}) = \frac{1}{2}\frac{x^2-y^2}{r^2}f(r)$, $\varphi_5(\mathbf{r}) = \frac{1}{2\sqrt{3}}\frac{3z^2-r^2}{r^2}f(r)$, where $f(r) = \frac{2\sqrt{2}}{3\sqrt{5}}(\frac{Z}{3a_B})^{3/2}(\frac{Zr}{3a_B})^2 e^{-Zr/3a_B}$. The choice of the $\mathbf{K}_i$ vectors is dictated by the symmetry of the Brillouin zone. The $\mathbf{K}_i$ vectors represent all difference vectors between equivalent symmetry points within $\frac{1}{48}$ of the Brillouin zone. In the fcc Brillouin zone (a truncated octahedron) the set of $\mathbf{K}_i$ vectors contains four elements: $\mathbf{K}_1 = (0,0,0)$, $\mathbf{K}_2 = (0,-2,0)\frac{2\pi}{a}$, $\mathbf{K}_3 = (-1,-1,-1)\frac{2\pi}{a}$, and $\mathbf{K}_4 = (-1,-1,1)\frac{2\pi}{a}$ (a is the lattice constant). These correspond to the difference vectors between a W point and its four equivalent points. In fcc crystals the other symmetry points do not yield new vectors. This is due to the symmetry properties of the truncated octahedron. In contrast to fcc Ni, the Brillouin zone of bcc iron is a rhombic dodecahedron. In iron one has to take into account seven $\mathbf{K}_i$ vectors: the connecting vectors of all six equivalent H points (for each fixed H point) and one extra $\mathbf{K}_i$ vector from the P point which is not contained in the set of connections of equivalent H points: $\mathbf{K}_1 = (0,0,0)$, $\mathbf{K}_2 = (-2,0,0)\frac{2\pi}{a}$, $\mathbf{K}_3 = (-1,-1,0)\frac{2\pi}{a}$, $\mathbf{K}_4 = (-1,1,0)\frac{2\pi}{a}$, $\mathbf{K}_5 = (-1,0,-1)\frac{2\pi}{a}$, $\mathbf{K}_6 = (-1,0,1)\frac{2\pi}{a}$, and $\mathbf{K}_7 = (0,-1,-1)\frac{2\pi}{a}$. All other connections of equivalent symmetry points (N for bcc and X, L, K, U for fcc) do not result in additional vectors $\mathbf{K}_i$. In Appendix B the Hamiltonian matrix elements for the band-structure calculation are shown.

Extending our previous nickel theory we perform a *weighted* three-dimensional summation over points in the irreducible $\frac{1}{48}$ of the Brillouin zone to correct for zone-boundary effects. The volume of every point at the boundary of the irreducible $\frac{1}{48}$ depends on the number of adjacent $\frac{1}{48}$ Brillouin-zone portions (e.g., each P point is weighted by $\frac{1}{24}$ since it involves 24 irreducible $\frac{1}{48}$ portions). The same procedure applies to all zone-boundary points.

We include the ferromagnetism of Fe by the exchange splitting of the diagonal matrix elements of the d bands ($E_{0\uparrow} \neq E_{0\downarrow}$). The s bands see this exchange splitting of the d bands via hybridization effects. Only pure s bands are not exchange split. The value of the exchange splitting J is taken from experiment, see Refs. 21 and 22. Furthermore, in order to obtain agreement with the observed d-band and s-band widths we reduce all hopping parameters (with respect to the values taken by Baker and Smith[20] by 40%) and shift the bottom of the s band (by 1.03 eV). In agreement with Argyres[23] we use for the spin-orbit coupling constant in iron the value of $\lambda_{s.o.} = 0.05$ eV. All other parameters are taken from Ref. 20.

III. RESULTS

We perform the calculation for the nonlinear magneto-optical Kerr susceptibility $\chi^{(2)}(\omega)$ in iron in order to com-

TABLE I. Parameters used for the calculation of the magneto-optical susceptibilities.

β	= 2.5 eV	A_1	= 0.0774 eV	B_1	= 20.57 eV
α	= 0.315 eV	A_2	= -0.00816 eV	B_2	= 18.28 eV
V_1	= 1.40 eV	A_3	= -0.1074 eV	E_0	= 9.646 eV
V_2	= 2.15 eV	A_4	= -0.2016 eV	Δ	= 0.068 eV
S	= 15.54 eV	A_5	= 0.1272 eV	J_0	= 1.78 eV
R	= 2.48×10^{-9}	A_6	= -0.0756 eV	$\lambda_{s.o.}$	= 0.05 eV
		A_7	= $A_3 - A_5 - \frac{\sqrt{3}}{2}A_6$	$\hbar\alpha_1$	0.1 / 0.4 eV

pare directly with experiment. The nonlinear and linear susceptibilities are determined via Eqs. (2) and (3). For the calculations we use the parameters listed in Table I.

To demonstrate the validity of the electronic structure used in our calculations of $\chi^{(1)}(\omega)$ and $\chi^{(2)}(\omega)$ (calculated with the parameters given in Table I), we show in Fig. 1 the resulting ferromagnetic band structure of Fe and compare with the results obtained from the spin-polarized version of the paramagnetic band structure in Ref. 20. The position of the Fermi level was calculated self-consistently for both cases by fixing the total number of conduction electrons: $N_{el} = 8$. To judge the quality of our band structure note that we obtain good agreement with *ab initio* calculations by Wang and Callaway[24] and by Hathaway, Jansen, and Freeman[25] if we use the *un*modified parameters (of Ref. 20). To obtain the observed d-band width we reduce as mentioned already the tight-binding hopping parameters A_i ($i = 1, \ldots, 7$). The points a, b, and c indicate the shift of the respective pure d-like or sd-hybridized high-symmetry points. Similarly, the modification of the energies β of the Γ point leads to a shift of the s-like symmetry points. This becomes most pronounced for the shift of the Γ point indicated by point d in Fig. 1. Note that we include the effects of ferromagnetism only via the spin-splitting of the d bands. Thus our calculation yields a spin splitting of the various bands according to their different sd hybridization. Note, as aimed we have very good agreement with the experimentally observed d-band width (3.1 eV for the occupied portion at point P, see Ref. 22).

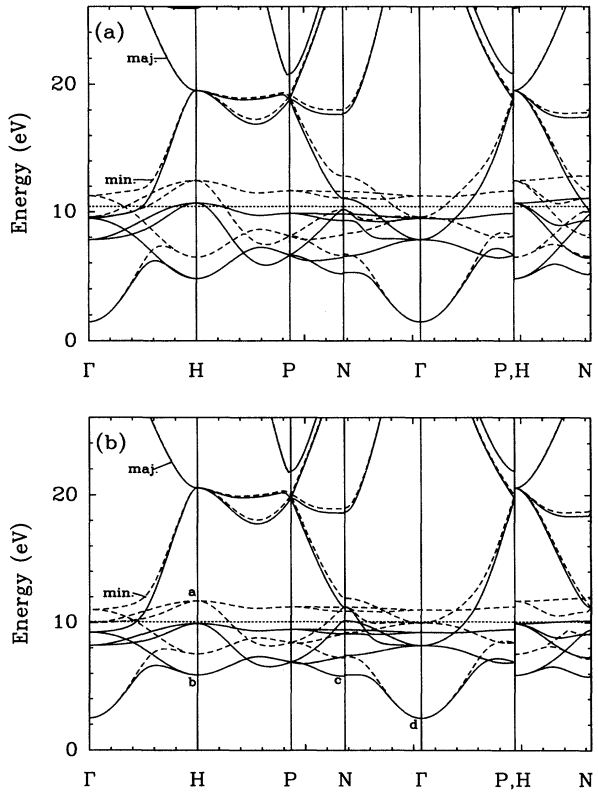

FIG. 1. Spin-polarized band structure of iron calculated within the combined interpolation scheme using parameters (a) given in Ref. 20 and (b) given in Table I. Solid curves refer to the majority-spin bands and dashed curves to the minority-spin bands. Note, the energy shifts in particular at (a), (b), (c), and (d).

Figure 2 shows the nonlinear magneto-optical Kerr susceptibility $\omega^2 \mathrm{Im}\chi^{(2)}_{xzz}(\omega)$ for Fe as a function of frequency ω. Note, $\omega^2 \mathrm{Im}\chi^{(2)}_{xzz}(\omega)$ for Fe is of the order of ($10^{16}\,\mathrm{s}^{-2}\,\mathrm{m/V}$) which is of similar magnitude as for nickel. The low-energy part of the spectrum (energy below 10 eV) consists of a minimum at 2.8 eV with $\omega^2 \mathrm{Im}\chi^{(2)}_{xzz}(\omega) < 0$ and two peaks at 4.5–6.0 eV and at 7.8 eV. A reduction of the damping constant $\hbar\alpha_1$ from 0.4 eV (dashed curve) to 0.1 eV (solid curve) reveals a large variety of secondary structure. In particular, the minimum is split into two subminima. The shoulder at approximately 1.3 eV, which becomes more pronounced

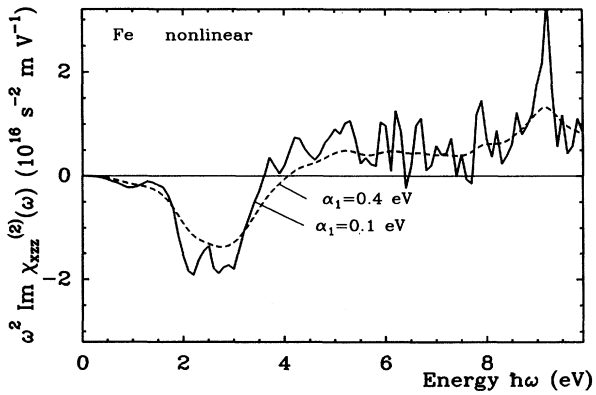

FIG. 2. Nonlinear magneto-optical Kerr susceptibility $\omega^2 \mathrm{Im}\chi^{(2)}_{xzz}(\omega)$ for the surface of ferromagnetic iron with in-plane magnetization M_y as a function of frequency ω. The dashed curve shows results using a resolution factor $\hbar\alpha_1 = 0.4$ eV; the solid line refers to $\hbar\alpha_1 = 0.1$ eV.

for the smaller value of $\hbar\alpha_1$, corresponds to the first peak at 0.6 eV in the nonlinear Kerr spectrum of nickel. To understand the physical origin of this structure, we analyze its dependence on the spin-dependent electron density of states, *sd* hybridization, and bandwidth in the following paragraph.

In Fig. 3 the minority- (dashed) and majority-spin electron contributions (dotted) to the nonlinear [3(a)] and linear [3(b)] magneto-optical susceptibilities (solid lines) are shown. It becomes clear that most of the contributions to the spectra at low frequencies result from the minority spins. The crossover from a dominating minority-spin to majority-spin contribution is at 4 eV for the nonlinear and at 7 eV for the linear Kerr spectrum. Thus, minority spins dominate the spectra over the entire range of visible light in agreement with Krinchik's observation.[9] Nevertheless, the influence of majority electrons is not negligible for the height of the first structure, especially for the linear Kerr spectrum. This behavior is in pronounced contrast to the situation in nickel, where only minority spins contribute to the low-energy part of the spectra ("strong ferromagnetism"). For comparison with nickel, see also Ref. 26.

The comparison of the nonlinear and linear magneto-optical spectra of iron leads to the general picture that the nonlinear Kerr spectrum is to some extent the derivative of the linear spectrum. The peaks of the nonlinear Kerr spectrum are shifted to lower energies compared with the linear spectrum. This behavior reflects the occurrence of energy denominators with frequencies ω and 2ω in the nonlinear magneto-optical susceptibility which also lead to more secondary structures in the nonlinear spectrum. Moreover, the linear majority- and minority-spin-decomposed contributions to $\omega^2 \mathrm{Im}\chi^{(1)}(\omega)$ keep the same sign, which is a consequence of linear-response theory and does not hold for the nonlinear spin-projected spectra. Thus, the spin-resolved contributions to the linear Kerr spectrum can be considered as results from a convoluted density of states for majority and minority electrons, respectively.

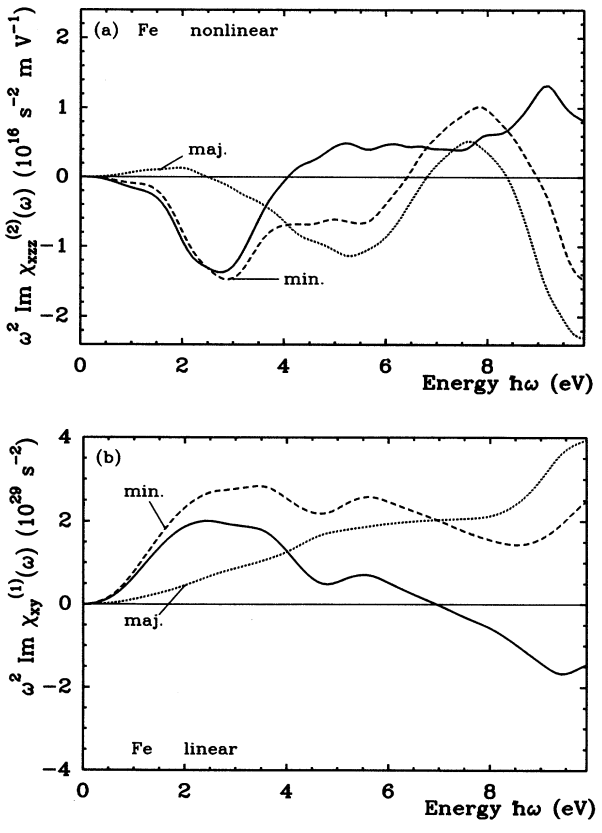

FIG. 3. (a) Nonlinear and (b) linear magneto-optical Kerr susceptibilities of Fe as functions of frequency ω (solid curves). The dashed curves refer to the minority-spin (min.) and the dotted curves to the majority-spin contribution (maj.).

The most striking difference between the nonlinear Kerr spectrum and the linear one is the drastic reduction of the susceptibility by 13 to 14 orders of magnitude. This reduction is easily understood by two pronounced differences. (i) The nonlinear magneto-optical tensor contains three dipole-transition matrix elements instead of two dipole matrix elements in the linear susceptibility which reduces the tensor magnitude by 11 orders. (ii) The remaining difference of 2 to 3 orders of magnitude results from the surface sensitivity of the nonlinear magneto-optical Kerr effect which leads to the prefactor $q_\parallel a$ in $\chi^{(2)}_{xzz}(\omega)$ ($q_\parallel a = 3.38 \times 10^{-3}$ for $q_\parallel = 1.181 \times 10^5$ cm^{-1}, corresponding to the experimental wavelength of 532 nm and the lattice constant $a = 2.86 \times 10^{-10}$ m of Fe).

In Fig. 4 we show the nonlinear [4(a)] and linear [4(b)] magneto-optical Kerr spectra for different values of the Fletcher-Wohlfahrt parameters. For the dotted curves, we use the values of the hopping parameters A_i ($i = 1, \ldots, 7$) given in Ref. 20. The dashed and solid curves correspond to a reduction of all A_i to 80% and 60% of these values, respectively. This reduction of the *d-d* hopping leads to a narrowing of the *d* band (see Fig. 1) which may partly simulate the non-negligible effects of electron-electron interactions. Due to such correlations the probability of transitions with lower energies is increased. This essentially leads to a shift of the first structures in the linear and nonlinear Kerr spectra to lower energies (by 0.5 and 0.3 eV for $0.8A_i$ and by 0.9 and 0.4 eV for $0.6A_i$, respectively) and to a simultaneous reduction of their heights. The second structure is affected less drastically: in the nonlinear spectrum, the shift towards lower energies is 0.2 eV for $0.8A_i$ and 0.3 eV for $0.6A_i$ and the peak height increases whereas the second peak of the linear spectrum decreases and is shifted to lower energies by 0.3 eV and 0.4 eV for $0.8A_i$ and $0.6A_i$, respectively. The shift of the second structures is due to transitions between the *d* band and *s*-like or *sd*-hybridized bands and is therefore always smaller than the shift of the first structures which predominantly result from transitions between *d*-like bands close to the Fermi level. The modifications of the third structure in the nonlinear and linear spectra increasingly correspond to bands far from the Fermi level and do not show a clear dependence on the *d-d* hopping elements. Thus, in summary we may conclude that changes in the *d*-band width affect different parts of the spectra, both linear and non-

linear ones, differently. We expect then such a behavior also with respect to changes in the position of the s band as can be seen in Fig. 5.

Figure 5 shows the nonlinear and linear magneto-optical spectrum for different values of the bottom of the s band (Γ point). The position β of the energy at the Γ point is increased from 1.47 eV via 2.0 eV and 2.5 eV to 3.0 eV. In the low-energy part of the spectra (below 8 eV), this shift accounts for the decreasing s-band width due to electron-electron interactions. Changing β affects, in particular, the first peak of the nonlinear spectrum and the second peak of the linear spectrum. These are shifted to smaller energies. The peaks at large energies (above 8 eV and 8.5 eV in the nonlinear and linear spectrum, respectively), however, are shifted to larger frequencies since the top of the s band lies at increasingly higher energies (high above the Fermi level). Thus, transitions from occupied levels into these unoccupied states occur at higher energies. Note that the first peak of the linear Kerr spectrum is mainly independent of β which is in agreement with our previous observation (see Fig. 4) that this peak involves mostly d-d transitions.

In Fig. 6 we compare the calculated *linear* Kerr spectra with experiment to find the best set of parameters

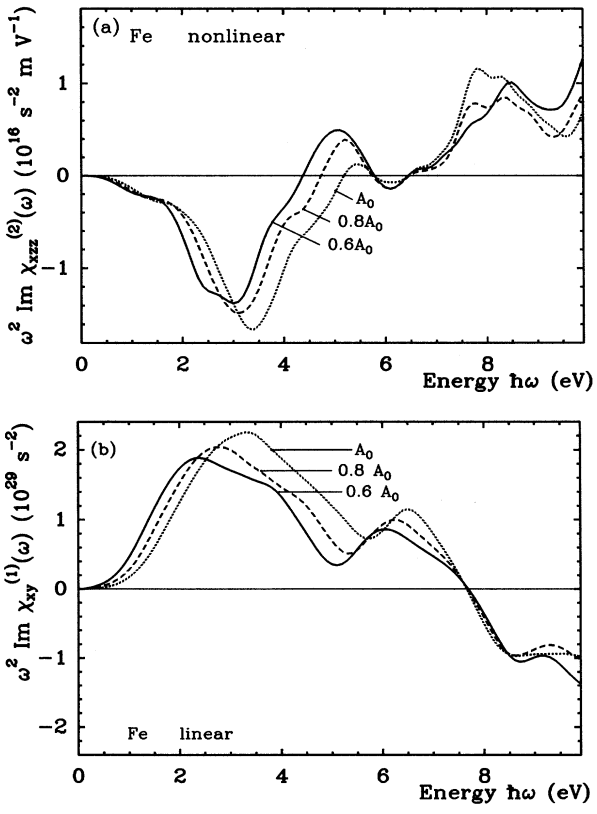

FIG. 4. (a) Nonlinear and (b) linear magneto-optical Kerr susceptibilities of Fe for different d-band widths as functions of frequency ω. The hopping parameters A_i ($i = 1, \ldots, 7$) are those of Ref. 20 (dotted line). The dashed and solid curves correspond to reduced values of 80% and 60% of the bandwidth used in Ref. 20, respectively.

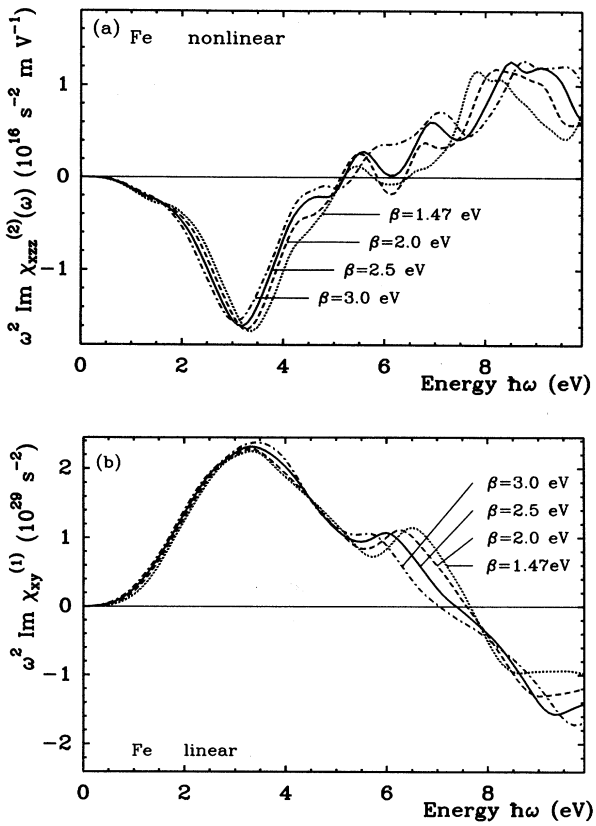

FIG. 5. Frequency dependence of the (a) nonlinear and (b) linear magneto-optical Kerr susceptibilities of Fe for shifted s bands (β is the energy of the Γ point).

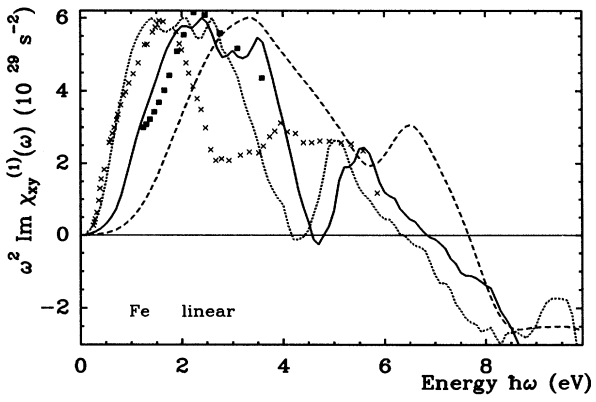

FIG. 6. Linear magneto-optical Kerr susceptibility $\omega^2 \mathrm{Im}\chi_{xy}^{(1)}(\omega)$ of Fe as a function of energy $\hbar\omega$ using the same parameters as in Ref. 20 (dashed curve) and for parameter values leading to the closest agreement with experimental results by Ferguson and Romagnoli (Ref. 10), given by squares (A_i = 60% of the values of Ref. 20 and β = 2.5 eV, solid curve). The crosses refer to experiments by Krinchik (Ref. 9). In order to reproduce these experimental results in our calculation we have further reduced the hopping parameters to A = 30% of the values given in Ref. 20 and obtain the results of the dotted curve.

for the calculations. We find the best agreement with the experimental peak position observed by Ferguson[10] for the following choice of parameters: $A_i = 60\%$ of the hopping parameters A_i used for the band-structure calculation by Baker and Smith[20] and $\beta = 2.5$ eV (solid line) (see also Ref. 27). This is interesting, since it seems to justify our assumption of appreciable d- and s-band narrowing due to electronic correlations. A further decrease of the d-band width is expected in two-dimensional magnetic structures as a consequence of the increased significance of correlations and reduction of atomic coordination number. In this manner, we are able to simulate the behavior in thin films. The dashed curve shows the spectrum for the unmodified parameters of Ref. 20 as used for band-structure calculations and gives peaks shifted towards higher energies by more than 1 eV. Thus, the use of the above band-structure-derived parameters is not sufficient to explain the linear magneto-optical Kerr spectrum of Fe. Nevertheless, the deviations are not as large as in the case of Ni, where usual calculations using *ab initio* band-structure results give completely wrong (peak) structures. It should be noted that our results for Fe are also in fair agreement with recent calculations of the linear Kerr spectrum by Oppeneer *et al.*[15] Note, they have used for the microscopic conductivity tensor the formula of Wang and Callaway[16] which is compared with our expression in Appendix A. Differences may result from different treatment of electron-electron interactions.

In Fig. 7 we show the dependence of the nonlinear [7(a)] and linear [7(b)] Kerr spectra on the exchange coupling constant J. In contrast to earlier work[12] we find for the linear spectrum (at least for energies below 7 eV) a monotonic increase of the peak heights with increasing J. As is shown in the inset, this increase starts linearly in J. For larger values of the exchange interaction, the dependence tends to saturate. The same holds for the first minimum in the nonlinear spectrum [see the inset of Fig. 7(a)]. In Appendix C we prove that the nonlinear and linear magneto-optical susceptibilities are linear in J for small J and then saturate for larger J. This holds for itinerant as well as for a more atomlike ferromagnetic behavior.

Our results for $\chi^{(2)}_{xzz}(\omega)$ can be used now to analyze the experimental results observed for Fe for the ratio $\frac{\chi^{(2)}_{\rm mag}(\omega)}{\chi^{(2)}_{\rm nonmag}(\omega)}$ of the magnetic and nonmagnetic nonlinear magneto-optical susceptibilities. We discuss this in the next section.

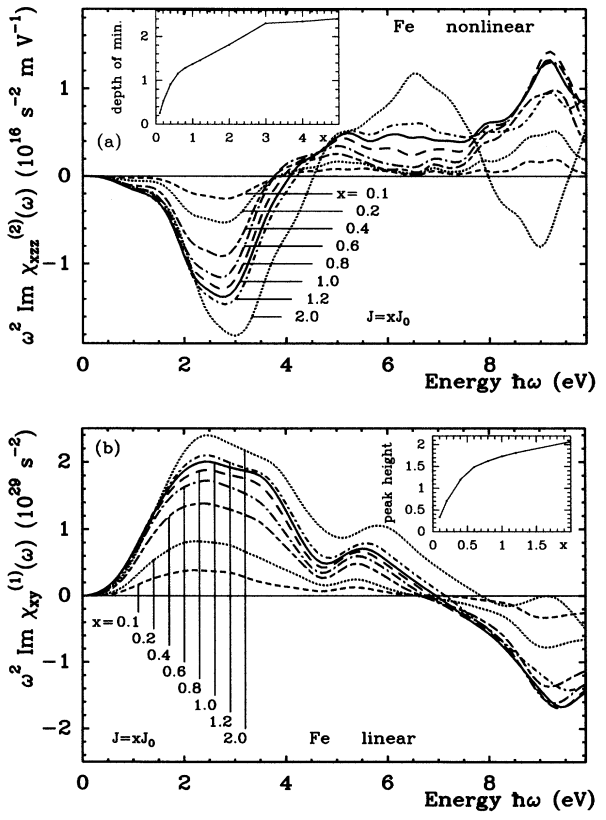

FIG. 7. Dependence of the (a) nonlinear and (b) linear magneto-optical Kerr susceptibilities of Fe on magnetization as characterized by the exchange splitting $J = xJ_0$, $J_0 = 1.78$ eV. The insets show the height of the first structure (at 2–3 eV) as a function of the exchange splitting.

IV. DISCUSSION

In view of our results presented in Sec. III it is possible to understand more about the differences in the Kerr spectrum expected for different ferromagnetic metals.

First, the dependence on J may be understood as follows. The increase of J has basically three effects: (i) Starting with small values of J the difference of allowed majority and minority electron dipole transitions at a certain frequency increases linearly in J, see illustration Fig. 8 in Appendix C. For large J, however, this difference saturates, since the self-consistently determined Fermi level becomes pinned and moves rigidly upon further increase of J (see Appendix C). (ii) As long as the increase of J and the subsequent self-consistent readjustment of the Fermi level do not cause bands to cross the Fermi energy, the overall shape and peak structure of the spectrum remains unaltered. As soon as Fermi-level crossings occur (either gradually for relatively steep bands or more abruptly for rather flat bands), the occupation character of the bands is changed, thus opening up new previously forbidden channels for electronic dipole transitions or closing previously allowed channels; see Fig. 8. This effect becomes noticeable if more than one electron per atom is transferred from one band to another. As a consequence, one may get drastic changes in the structure of the nonlinear and linear Kerr spectra. This is in particular the case if all transitions contributing to a pronounced structure change. Although the value of J in ferromagnetic Fe is 1.78 eV, which is quite large, this possibility occurs only for energies larger than 7 eV and for a value $J = 2J_0$. Otherwise the features of the spectra appear to be very robust. (iii) As is shown in detail in Appendix C, the increase of J leads also to a small shift of the peak energies to larger values. This is in particular so for the first structure of the nonlinear and linear Kerr spectrum. The

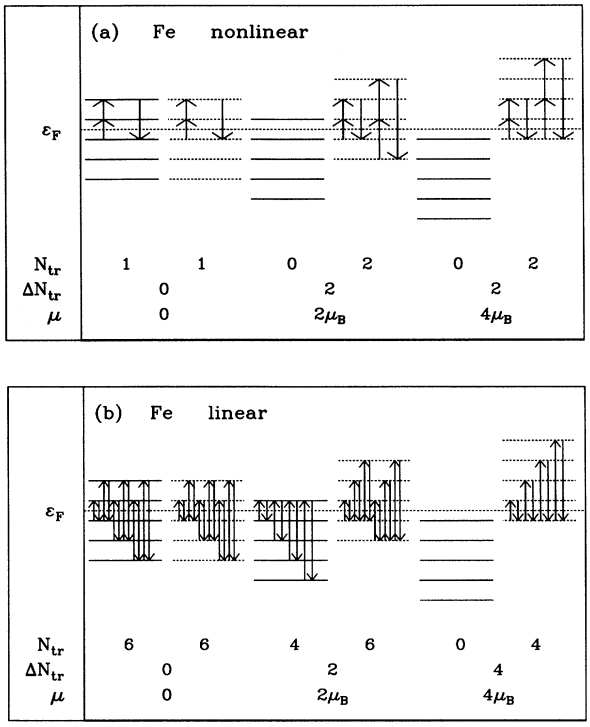

FIG. 8. Illustration of the d-band transitions in Fe in an atomic picture. (a) refers to the nonlinear case and (b) to the linear case. Here ε_F, μ, N_{tr}, ΔN_{tr} denote the Fermi energy, magnetic moment, number of transitions, and difference of transitions in minority- and majority-spin bands, respectively.

reason is that the exchange splitting of the d-like bands affect differently the s-like and sd-hybridized states via sd hybridization. This explains also the larger shift of the second structure which is due to s-d transitions, in the linear (and to some extent also in the nonlinear) spectrum compared to the shift of the first structure. Note, in general these shifts are relatively small and thus do not change the overall features of the spectra.

Second, concerning the dependence of the spectra on spin-orbit coupling one should note the following: the nonlinear magneto-optical Kerr spectrum depends linearly on spin-orbit coupling. This does not only hold for our perturbational treatment of spin-orbit interaction, but is also true if this interaction is included in the diagonal (L_zS_z) and off-diagonal matrix elements [$L_xS_x + L_yS_y = \frac{1}{2}(L_+S_- + L_-S_+)$] of the Hamiltonian.[12,28] These general features of the theory are of interest for a systematic understanding of the Kerr effect in the transition-metal series and will also be useful for the comparison of the Kerr spectra of Ni and Fe.

Next, we compare the calculated nonlinear magneto-optical Kerr spectra of Fe with those obtained previously for Ni (see Ref. 5). Of course, it matters that the electronic structure of bcc Fe and fcc Ni is different. For the Fe spectra, a detailed calculation of the weight of boundary points of the Brillouin zone is performed for the **k**-space summation yielding the Kerr spectra. Such weights were not included in the Ni spectra calculation. Thus, for the comparison of Fe and Ni spectra we determined for Ni a weight factor $F = 1.33$ for the boundary points. Thus we obtain for Fe and Ni for the structure at 2–3 eV a height ratio $\frac{P_{Fe}}{P_{Ni}}F$ of 2.2–2.5 (rather than 1.7–1.9 for $F = 1$). Note, the height ratio is not simply given by the ratio of the exchange couplings (4.5), or that of the magnetic moments (3.8), but also by the difference of spin-orbit coupling which enhances relatively the height of the Ni spectra ($\lambda_{s.o.}$[Fe] = 50 meV and $\lambda_{s.o.}$[Ni] = 70 meV). The larger minima and maxima in the nonlinear magneto-optical Kerr spectrum of Fe compared with Ni (and similarly for the linear spectra) result mainly for two reasons. (i) The exchange splitting is larger in Fe by a factor of 4.5 (compared to 400 meV for the t_{2g} orbitals of Ni). Here, however, it plays a role that the J dependence of the Kerr effect tends to saturate for large values of J. (ii) The filling of the $3d$ bands is different. Fe is much closer to half-filling which leads to a larger number of d-d transitions. Thus, it is clear that the maxima and minima in the nonlinear (and linear) magneto-optical spectrum are more pronounced for Fe than for Ni. Furthermore, the peaks and minima in the optical region of Fe are shifted to higher energies compared to Ni because of the larger width of the Fe d band. This discussion shows how the Kerr spectra change from transition metal to transition metal.

Finally, we should remark on using constant matrix elements for Fe in contrast to Ni. The calculations of the MOKE and NLMOKE spectra for nickel have been performed by using **k**-dependent as well as constant matrix elements.[5] A detailed comparison of the results shows that there is no difference in the overall shape of the linear and nonlinear Kerr spectra. In general, however, the peaks become narrower for the **k**-dependent matrix elements due to the additional selection rules introduced by these dipole transition-matrix elements. The peak-height ratios and the peak-width ratios are only marginally improved by the **k** dependence of the matrix elements. On the other hand, the peaks obtained for momentum-independent matrix elements are smoothed out due to the averaging over many dipolar transitions for a fixed frequency. This effect seems to comply more with the situation in solids where the selection rules for single transitions become less important. In experiment, the peaks are broadened by the finite resolution of the apparatus and by the artificial diaphragm in the synchrotron beam. Besides, theoretical spectra are usually smoothed by a damping factor between 0.4 eV and 0.68 eV.[14,15] Thus, it is more physical to perform the calculations for iron using constant matrix elements to obtain peak widths in accordance with the experimental peaks.

It is interesting to comment on our use of a parametrized band structure. This offers three advantages. (i) It allows for the simple and efficient incorporation of experimentally accessible parameters which can be deduced from several independent measurements such as photoemission, inverse photoemission, the de Haas–van Alphen effect, or various spin-polarization spectroscopies and many-body theories. This is necessary in view of the pronounced deviations of the experimentally observed d-band widths and exchange splittings[22] from

TABLE II. Angle-resolved photoemission data, see Ref. 22.

Ratio (theory/experiment) of	Fe	Co	Ni
Exchange splitting	1.0	1.2	2.2
Width of occupied d band	1.1	1.2	1.45

the predictions of *ab initio* theories in ferromagnetic transition metals (see Table II). The increasing discrepancy (from Fe to Ni) shows that many-body effects play a less important role in iron, as compared with cobalt or nickel. This is consistent with the crystal structure of these materials: in bcc iron the atomic density is lower than in fcc nickel. The Ni fcc structure has the largest packing density and the most pronounced many-body effects in the partly filled d bands. The combined interpolation scheme is an efficient way to account for the most important many-body effects which are essential for the spin-polarized, magneto-optically excited states probed most sensitively by NLMOKE and MOKE. (ii) The parametrization amounts to introducing control parameters and their variation helps us to understand how they determine the various features of the nonlinear (and linear) Kerr spectra and thus to understand their physical origin. (iii) The parametrization will be very useful for applications to thin films or alloys.

We use now the previous general theoretical considerations for the comparison of the theory with the experiment of Reif *et al.*[6] The main experimental results obtained for only one frequency ($\hbar\omega = 2.33$ eV) can be summarized as follows: Upon reversing the direction of the in-plane surface magnetization by the external magnetic field one observes for $\delta = I(\mathbf{M}) - I(-\mathbf{M})$ a large value. Here I refers to the SHG intensity and $\mathbf{M}$ to the in-plane magnetization at the surface. Using $I \sim P^2$, $P = \chi^{(2)}E^2$ [see Eq. (1)], and $\chi^{(2)}_{\pm} = \chi^{(2)}_{\text{nonmag}} \pm \chi^{(2)}_{\text{mag}}$, one may write

$$\frac{\delta}{I_{\text{nonmag}}} = \frac{[\chi^{(2)}_{+}]^2 - [\chi^{(2)}_{-}]^2}{[\chi^{(2)}_{\text{nonmag}}]^2} = \frac{4\chi^{(2)}_{\text{mag}}\chi^{(2)}_{\text{nonmag}}}{[\chi^{(2)}_{\text{nonmag}}]^2} = 4\frac{\chi^{(2)}_{\text{mag}}}{\chi^{(2)}_{\text{nonmag}}}.$$

Thus, one finds from experiment (which determines $\frac{\delta}{I_{\text{nonmag}}}$) a value of $\frac{\chi^{(2)}_{\text{mag}}}{\chi^{(2)}_{\text{nonmag}}} = 0.25$. Also experiment confirms the theoretically predicted sensitivity of the nonlinear Kerr effect for surface magnetism, since upon CO chemisorption δ disappears exponentially with time t and since $\chi^{(2)}_{\text{nonmag}}(t) \approx$ const. Furthermore, increasing the laser intensity causes $\delta \longrightarrow 0$. Note, the Kerr angle was not determined experimentally.

Regarding these experimental findings we note the following: First, the observability of the nonlinear Kerr effect was predicted theoretically by Hübner and Bennemann[1,2] and by Pan, Wei, and Shen.[3] We estimate $\frac{\chi^{(2)}_{\text{mag}}}{\chi^{(2)}_{\text{nonmag}}}$ for Fe as follows:

$$\left(\frac{\chi^{(2)}_{\text{mag}}}{\chi^{(2)}_{\text{nonmag}}}\right)_{\text{Fe}} = \left(\frac{\chi^{(2)}_{\text{mag}}}{\chi^{(2)}_{\text{nonmag}}}\right)_{\text{Ni}} \frac{\chi^{(2)}_{\text{mag,Fe}}}{\chi^{(2)}_{\text{mag,Ni}}} \approx \left(\frac{\chi^{(2)}_{xzz}}{\chi^{(2)}_{zzz}}\right)_{\text{Ni}} \frac{\chi^{(2)}_{xzz,\text{Fe}}}{\chi^{(2)}_{xzz,\text{Ni}}} \approx \left(\frac{\lambda_{\text{s.o.}}}{\hbar\omega}\right)\frac{p_{\text{Fe}}}{p_{\text{Ni}}}F = 0.07 \times 2.5 = 0.175.$$

Here, we take the same $\chi^{(2)}_{\text{nonmag}}$ for Fe and Ni which seems plausible, also in view of the optical-absorption experiments and the linear magneto-optical Kerr effect.[15] Also, we use for the case of p polarization and grazing incidence with $\chi^{(2)}_{\text{mag}} \approx \chi^{(2)}_{xzz}$ and $\chi^{(2)}_{\text{nonmag}} \approx \chi^{(2)}_{zzz}$ the approximation

$$\left(\frac{\chi^{(2)}_{\text{mag}}}{\chi^{(2)}_{\text{nonmag}}}\right)_{\text{Ni}} \approx \left(\frac{\chi^{(2)}_{xzz}}{\chi^{(2)}_{zzz}}\right)_{\text{Ni}} \approx \left(\frac{\chi^{(2)}_{zzz}}{\chi^{(2)}_{zzz}}\right)_{\text{Ni}} \left(\frac{\lambda_{\text{s.o.}}}{\hbar\omega}\right) = \left(\frac{\lambda_{\text{s.o.}}}{\hbar\omega}\right) = 0.07.$$

This approximation,[6,29] which is valid for Ni with a full majority band, does not hold for Fe. Finally, the factor $\frac{\chi^{(2)}_{\text{mag,Fe}}}{\chi^{(2)}_{\text{mag,Ni}}}$ is approximated by the ratio of the peak heights discussed earlier in this section,

$$\frac{\chi^{(2)}_{\text{mag,Fe}}}{\chi^{(2)}_{\text{mag,Ni}}} \approx \frac{\chi^{(2)}_{xzz,\text{Fe}}}{\chi^{(2)}_{xzz,\text{Ni}}} \approx \frac{p_{\text{Fe}}}{p_{\text{Ni}}}F \approx 2.5.$$

As already pointed out before in this paper, this value results not only from scaling with the magnetic moments as was previously assumed for the analysis of the experiment.[6,30,31] It is remarkable that our estimate for $\frac{\chi^{(2)}_{\text{mag}}}{\chi^{(2)}_{\text{nonmag}}} \approx \frac{\delta}{I_{\text{nonmag}}}$ is in such good agreement with the experimental value.

The surface sensitivity of the nonlinear Kerr effect is in accordance with the theoretical prediction. Theory yields that SHG occurs only for a few atomic layers at the surface where inversion symmetry is broken. Thus we are inclined to interpret the disappearance of δ upon CO chemisorption as resulting from vanished surface magnetization. The band structure should change only weakly upon the chemisorption of CO. Thus $\chi^{(2)}_{\text{nonmag}}(t) \approx$ const is in accordance with the experimental observation. This interpretation is supported by SHG experiments on CO chemisorbed at Pt(111) at $\lambda = 532$ nm (see Ref. 32).

Note, magnetism may also be destroyed by atomic disorder. Thus the nonlinear Kerr effect may disappear when the laser intensity is increased. Finally, theory permits a nonlinear Kerr effect in principle also for coated surfaces and for interfaces and, furthermore, does not require saturated magnetization.[33] This indicates that our

theory is able to explain the main experimental observations.

V. SUMMARY

We have presented a microscopic theory which may be used for a systematic understanding of the nonlinear magneto-optical Kerr effect in transition metals. In particular, we have given results for the dependence of the nonlinear Kerr spectrum on *s*- and *d*-band widths, *sd* hybridization, exchange interaction, spin-orbit coupling, and crystal structure (fcc Ni vs bcc Fe). The theory is used to analyze recent NLMOKE experiments in Fe. The theory may be extended to thin films. Calculations are in progress.

ACKNOWLEDGMENTS

Stimulating discussions with J. Kirschner, E. Matthias, and J. Reif are gratefully acknowledged.

APPENDIX A: DERIVATION OF THE SUSCEPTIBILITIES

Following the derivation by Ehrenreich and Cohen[17] the frequency-dependent dielectric function was found in the self-consistent-field approach,

$$\varepsilon(\mathbf{q},\omega)=1-\lim_{\alpha\to 0}\frac{4\pi e^2}{q^2\Omega}\sum_{\mathbf{k},l,l'}|\langle\mathbf{k}l|e^{-i\mathbf{q}\cdot\mathbf{r}}|\mathbf{k}+\mathbf{q},l'\rangle|^2\times\frac{f(E_{\mathbf{k}+\mathbf{q},l'})-f(E_{\mathbf{k}l})}{E_{\mathbf{k}+\mathbf{q},l'}-E_{\mathbf{k}l}-\hbar\omega+i\hbar\alpha}. \quad \text{(A1)}$$

We have taken into account magnetism via the spin dependence of the electronic energies and wave functions and a summation over the spin directions. We include the spin-orbit interaction within first-order Heitler-Ma perturbation theory. Applying the procedure used by Cohan and Hameka[34] for gases and liquids, the product of matrix elements (two in the linear case and three in the nonlinear case) changes due to the perturbation in one wave function. The perturbation of the dipole operators may be neglected (see also Kittel[35]). Collecting all first order terms, i.e., those resulting from the perturbation of one wave function only (and unperturbed other parts of the matrix elements) one finds a sum of the form (for the linear case)

$$\sum_{\mathbf{k_1}}\frac{V_{\mathbf{k_1};\mathbf{k}+\mathbf{q},l'\sigma}[\mathbf{k_1}\times(\mathbf{k}+\mathbf{q})\langle\boldsymbol{\sigma}\rangle]}{E_{\mathbf{k}+\mathbf{q},l'\sigma}-E_{\mathbf{k_1}}}\langle\mathbf{k_1}|e^{i\mathbf{q}\cdot\mathbf{r}}|\mathbf{k}l\sigma\rangle\times\langle\mathbf{k}l\sigma|e^{-i\mathbf{q}\cdot\mathbf{r}}|\mathbf{k}+\mathbf{q},l'\sigma\rangle, \quad \text{(A2)}$$

where $V_{\mathbf{k_1};\mathbf{k}+\mathbf{q},l'\sigma}$ is the full crystal potential matrix element and $\langle\mathbf{k_1}|$ denotes the perturbed wave function. The sum over $\mathbf{k_1}$ can be simplified considerably. First, the wave functions containing $\mathbf{k_1}$ can be replaced by the unperturbed ones. Second, the prefactor can be replaced as follows:

$$\sum_{\mathbf{k_1}}\frac{V_{\mathbf{k_1};\mathbf{k}+\mathbf{q},l'\sigma}[\mathbf{k_1}\times(\mathbf{k}+2\mathbf{q})\langle\sigma\rangle]}{E_{\mathbf{k}+\mathbf{q},l'\sigma}-E_{\mathbf{k_1}}}\approx\frac{\lambda_{\text{s.o.}}}{\hbar\omega-\lambda_{\text{s.o.}}}\approx\frac{\lambda_{\text{s.o.}}}{\hbar\omega}, \quad \text{(A3)}$$

since $\lambda_{\text{s.o.}}\ll\hbar\omega$; see also the more-detailed discussion in Ref. 5. The perturbative treatment can be interpreted as replacing $\langle\mathbf{k}+\mathbf{q}|$ by $(\lambda_{\text{s.o.}}/\hbar\omega)\langle\mathbf{k}+\mathbf{q}|$ instead of $\sum_{\mathbf{k_1}}\frac{V_{\mathbf{k_1};\mathbf{k}+\mathbf{q},l'\sigma}[\mathbf{k_1}\times(\mathbf{k}+\mathbf{q})\langle\boldsymbol{\sigma}\rangle]}{E_{\mathbf{k}+\mathbf{q},l'\sigma}-E_{\mathbf{k_1}}}\langle\mathbf{k_1}|$ [see Eqs. (A2) and (A3)].

By neglecting the spin indices the same result for the dielectric function [see Eq. (A1)] follows also directly from the Kubo formula for the current-current correlation function as was shown in detail by Haug and Schmitt-Rink.[18] Following their argumentation we show now that Eq. (A1) also contains the plasmon pole for the case of intraband transitions (see also Ref. 17). In the long-wavelength limit the matrix element can be rewritten as

$$\lim_{\mathbf{q}\to 0}\langle\mathbf{k}l|e^{-i\mathbf{q}\cdot\mathbf{r}}|\mathbf{k}+\mathbf{q},l'\rangle=\delta_{ll'}-i\langle\mathbf{k}l|\mathbf{q}\cdot\mathbf{r}|\mathbf{k}+\mathbf{q},l'\rangle(1-\delta_{ll'}). \quad \text{(A4)}$$

The first and second term refers to the intraband and interband contributions, respectively. Thus, the intraband contribution to the dielectric function is given by

$$\begin{aligned}
&1-\lim_{\mathbf{q}\to 0}\frac{4\pi e^2}{q^2}\sum_{\mathbf{k},l}\frac{f(E_{\mathbf{k}+\mathbf{q},l})-f(E_{\mathbf{k}l})}{E_{\mathbf{k}+\mathbf{q},l}-E_{\mathbf{k}l}-\hbar\omega-i\hbar\alpha}\\
&=1-\lim_{\mathbf{q}\to 0}\frac{4\pi e^2}{q^2}\sum_{\mathbf{k},l}[f(E_{\mathbf{k}+\mathbf{q},l})-f(E_{\mathbf{k}l})]\left\{\frac{-1}{\hbar\omega+i\hbar\alpha}-\frac{E_{\mathbf{k}+\mathbf{q},l}-E_{\mathbf{k}l}}{(\hbar\omega+i\hbar\alpha)^2}+\cdots\right\}\\
&\approx 1+\frac{4\pi e^2}{q^2}\sum_{\mathbf{k},l}[\mathbf{q}\cdot\nabla_{\mathbf{k}}f(E_{\mathbf{k}l})]\,(\mathbf{q}\cdot\nabla_{\mathbf{k}}E_{\mathbf{k}l})\,\frac{1}{(\hbar\omega+i\hbar\alpha)^2}\\
&=1-\frac{4\pi e^2}{q^2}\,\frac{q^2}{(\hbar\omega+i\hbar\alpha)^2}\sum_{\mathbf{k}l}f(E_{\mathbf{k}l})\frac{\partial^2E_{\mathbf{k}l}}{\partial\mathbf{k}^2}\\
&=1-\frac{4\pi e^2}{(\hbar\omega+i\hbar\alpha)^2}\sum_{\mathbf{k}l}\frac{f(E_{\mathbf{k}l})}{m_{\mathbf{k}l}}\\
&=1-\frac{\omega_{\text{pl}}^2}{(\omega+i\alpha)^2}, \quad \text{(A5)}
\end{aligned}$$

where $m_{\mathbf{k}l}$ is the effective mass tensor and $\omega_{\rm pl}$ is the plasma frequency. Decomposing the independent summation over l and l' in Eq. (A1) we obtain for the interband contribution to $\varepsilon(\mathbf{q},\omega)$

$$\lim_{\mathbf{q}\to 0}\frac{4\pi e^2}{q^2}\sum_{\mathbf{k}l,\mathrm{occ}}\sum_{\mathbf{k}l',\mathrm{unocc}}|\langle\mathbf{k}l|\mathbf{q}\cdot\mathbf{r}|\mathbf{k}+\mathbf{q},l'\rangle|^2\left(\frac{1}{E_{\mathbf{k}+\mathbf{q},l}-E_{\mathbf{k}l}-\hbar\omega-i\hbar\alpha}+\frac{1}{E_{\mathbf{k}+\mathbf{q},l}-E_{\mathbf{k}l}+\hbar\omega+i\hbar\alpha}\right), \tag{A6}$$

which is precisely the partial fraction decomposition of the result by Wang and Callaway,[16]

$$\lim_{\mathbf{q}\to 0}\frac{4\pi e^2}{q^2}\sum_{\mathbf{k}l,\mathrm{occ}}\sum_{\mathbf{k}l',\mathrm{unocc}}|\langle\mathbf{k}l|\mathbf{q}\cdot\mathbf{r}|\mathbf{k}+\mathbf{q},l'\rangle|^2\frac{2(E_{\mathbf{k}+\mathbf{q},l}-E_{\mathbf{k}l})}{(E_{\mathbf{k}+\mathbf{q},l}-E_{\mathbf{k}l})^2-(\hbar\omega+i\hbar\alpha)^2}. \tag{A7}$$

Thus, our result for the optical dielectrical function may be rewritten as

$$\varepsilon(\omega)=1-\frac{\omega_{\rm pl}^2}{(\omega+i\alpha)^2}-4\pi e^2\sum_{\mathbf{k}l,\mathrm{occ}}\sum_{\mathbf{k}l',\mathrm{unocc}}|\langle\mathbf{k}l|\mathbf{q}\cdot\mathbf{r}|\mathbf{k}+\mathbf{q},l'\rangle|^2\frac{2(E_{\mathbf{k}+\mathbf{q},l}-E_{\mathbf{k}l})}{(E_{\mathbf{k}+\mathbf{q},l}-E_{\mathbf{k}l})^2-(\hbar\omega+i\hbar\alpha)^2}, \tag{A8}$$

which after subtraction of unity and subsequent multiplication with $[i(\omega+i\alpha)]$ gives the formula for the optical conductivity given by Wang and Callaway[16] [see Eq. (5.5a) of Ref. 17], since

$$|\langle\mathbf{k}l|\mathbf{r}|\mathbf{k}+\mathbf{q},l'\rangle|^2=\frac{|\langle\mathbf{k}l|\mathbf{p}|\mathbf{k}+\mathbf{q},l'\rangle|^2}{m^2(E_{\mathbf{k}+\mathbf{q},l}-E_{\mathbf{k}l})^2}. \tag{A9}$$

APPENDIX B: MATRIX ELEMENTS OF THE HAMILTON OPERATOR

The Hamiltonian matrix elements for the s bands can be written as

$$\begin{aligned}H_{\mathbf{k}+\mathbf{K_i};\mathbf{k}+\mathbf{K_i}}&=\beta+\alpha|\mathbf{k}+\mathbf{K_i}|^2+Sj_2^2(|\mathbf{k}+\mathbf{K_i}|R),\\ H_{\mathbf{k}+\mathbf{K_i};\mathbf{k}+\mathbf{K_j}}&=F_i(\mathbf{k})F_j(\mathbf{k})\{V(|\mathbf{K_i}-\mathbf{K_j}|)+Sj_2(|\mathbf{k}+\mathbf{K_i}|R)j_2(|\mathbf{k}+\mathbf{K_j}|R)P_2[(\mathbf{k}+\mathbf{K_i})\cdot(\mathbf{k}+\mathbf{K_j})]\}.\end{aligned} \tag{B1}$$

The hybridization part has the following form:

$$H_{\mathbf{k}+\mathbf{K_i};\mu}=B_\mu F_i(\mathbf{k})j_2(|\mathbf{k}+\mathbf{K_i}|R)\varphi_\mu(\mathbf{k}+\mathbf{K_i}) \tag{B2}$$

with different constants $B_\mu=B_{t_{2g}}$ for $\mu=8,9,10$ and B_{e_g} for $\mu=11,12$ for orbitals of different symmetry (in contrast to the Ni theory) thus reflecting crystal-field splitting.

The d-band part was calculated in the three-center approximation by retaining the first- and second-nearest-neighbor interactions of the bcc lattice. Within the three-center approximation, we do not only incorporate the hopping integrals (as in the two-center approach) but also take into account crystal-field splitting. This might become important for future considerations of the magnetocrystalline anisotropy. Using Fletcher-Wohlfahrt parameters the matrix elements are given as

$$\begin{aligned}H_{8,8}&=E_0+2A_1(\cos 2\xi+\cos 2\eta)+2A_2\cos 2\zeta\\&\quad+8A_3\cos\xi\cos\eta\cos\zeta,\\ H_{8,9}&=-8A_7\sin\xi\cos\eta\sin\zeta,\\ H_{8,10}&=-8A_7\cos\xi\sin\eta\sin\zeta,\\ H_{8,11}&=0,\\ H_{8,12}&=-8A_6\sin\xi\sin\eta\cos\zeta,\\ H_{9,9}&=E_0+2A_1(\cos 2\eta+\cos 2\zeta)+2A_2\cos 2\xi\\&\quad+8A_3\cos\xi\cos\eta\cos\zeta,\\ H_{9,10}&=-8A_7\sin\xi\sin\eta\cos\zeta,\\ H_{9,11}&=-\sqrt{3}H_{9,12}=-4\sqrt{3}A_6\cos\xi\sin\eta\sin\zeta,\\ H_{10,10}&=E_0+2A_1(\cos 2\xi+\cos 2\zeta)+2A_2\cos 2\eta\\&\quad+8A_3\cos\xi\cos\eta\cos\zeta,\\ H_{10,11}&=\sqrt{3}H_{10,12}=4\sqrt{3}A_6\sin\xi\cos\eta\sin\zeta,\\ H_{11,11}&=E_0+\Delta+\tfrac{3}{2}A_4(\cos 2\xi+\cos 2\eta)\\&\quad+\tfrac{1}{2}A_2(\cos 2\xi+\cos 2\eta+4\cos 2\zeta)\\&\quad+8A_5\cos\xi\cos\eta\cos\zeta,\\ H_{11,12}&=\frac{\sqrt{3}}{2}(A_2-A_4)(\cos 2\xi-\cos 2\eta),\\ H_{12,12}&=E_0+\Delta+\tfrac{3}{2}A_2(\cos 2\xi+\cos 2\eta)\\&\quad+\tfrac{1}{2}A_4(\cos 2\xi+\cos 2\eta+4\cos 2\zeta)\\&\quad+8A_5\cos\xi\cos\eta\cos\zeta.\end{aligned} \tag{B3}$$

APPENDIX C: J DEPENDENCE OF THE SPECTRA

First, we calculate the J dependence of the peak position in the presence of sd hybridization. The exchange splitting of one d band and one sd band yields a different shift of majority- and minority-spin bands. The distances ΔE between the split bands depend on the exchange splitting value J,

$$\Delta E(\uparrow)=\sqrt{\left(E_1-E_2-\frac{J}{2}\right)^2+4V^2},$$

$$\Delta E(\downarrow)=\sqrt{\left(E_1-E_2+\frac{J}{2}\right)^2+4V^2},$$

where E_1 and E_2 are the original paramagnetic band positions and V describes the band hybridization.

Second, we calculate the J dependence of the linear magneto-optical Kerr spectrum consisting of one hypothetical peak of Lorentzian shape. Assuming a different J dependence for the majority- and minority-spin peaks, i.e., the majority- and minority-spin electrons undergo transitions between bands with different J dependence, the resulting linear Kerr susceptibility may be written in the following form:

$$\chi^{(1)} = \frac{AJ^2 + BJ}{CJ^2 + DJ + E},$$

where A, B, C, D, E are J-independent constants. For $J \to 0$ the susceptibility depends linearly on J, for $J \to \infty$ it tends to saturate.

The corresponding nonlinear spectrum consists of peaks whose shape is that of the derivative of a Lorentzian. The result for the J dependence of this nonlinear Kerr spectrum is

$$\chi^{(2)} \sim \frac{J^3 + aJ^2 + bJ}{J^3 + cJ^2 + dJ + e},$$

which again shows linear J dependence for small J and saturation behavior for large values of J.

Third, we calculate the J dependence of the linear and nonlinear magneto-optical Kerr spectra for Fe *atoms*. In Fig. 8 the atomic $3d$ bands of iron ($N_{\mathrm{Fe}} = 6$) are shown schematically. They cross the Fermi level with increasing exchange interaction. We obtain the number of possible transitions in majority- and minority-spin bands, the difference of which is a measure for the Kerr susceptibility. For a sufficiently large exchange interaction the bands no longer cross the Fermi level that demonstrates the case of saturation that occurs for smaller J in the nonlinear case compared to the linear one.

[1] W. Hübner and K. H. Bennemann, Europhys. Conf. Abs. **13A**, A42 (1989).

[2] W. Hübner and K. H. Bennemann, Phys. Rev. B **40**, 5973 (1989).

[3] Ru-Pin Pan, H. D. Wei, and Y. R. Shen, Phys. Rev. **39**, 1229 (1989).

[4] A. Vaterlaus, T. Beutler, and F. Meier, Phys. Rev. Lett. **67**, 3314 (1991).

[5] W. Hübner, Phys. Rev. B **42**, 11 553 (1990).

[6] J. Reif, J. C. Zink, C.-M. Schneider, and J. Kirschner, Phys. Rev. Lett. **67**, 2878 (1991).

[7] R. H. Victora and L. M. Falicov, Phys. Rev. Lett. **55**, 1140 (1985).

[8] W. Hübner and L. M. Falicov, Solid State Commun. **85**, 385 (1993).

[9] G. S. Krinchik and V. A. Artem'ev, Zh. Eksp. Teor. Fiz. **53**, 1901 (1967) [Sov. Phys. JETP **26**, 1080 (1968)]; J. Appl. Phys. **39**, 1276 (1968).

[10] P. E. Ferguson and R. J. Romagnoli, J. Appl. Phys. **40**, 1236 (1969).

[11] J. L. Erskine and E. A. Stern, Phys. Rev. Lett. **30**, 1329 (1973); J. L. Erskine, Physica **89B**, 83 (1977).

[12] D. K. Misemer, J. Magn. Magn. Mater. **72**, 267 (1988).

[13] S. V. Halilov and Yu. A. Uspenskii, J. Phys. Condens. Matter **2**, 6137 (1990).

[14] H. Ebert, Habilitations thesis, University of Munich, 1990.

[15] P. M. Oppeneer, T. Maurer, J. Sticht, and J. Kübler, Phys. Rev. B **45**, 10 924 (1992).

[16] C. S. Wang and J. Callaway, Phys. Rev. B **9**, 4897 (1974).

[17] H. Ehrenreich and M. H. Cohen, Phys. Rev. **115**, 786 (1959).

[18] H. Haug and S. Schmitt-Rink, Prog. Quantum Electron. **9**, 3 (1984).

[19] L. Hodges, H. Ehrenreich, and N. D. Lang, Phys. Rev. **152**, 505 (1966).

[20] S. K. Baker and P. V. Smith, J. Phys. F **7**, 781 (1977).

[21] Using angle-resolved photoemission spectroscopy Eastman, Himpsel, and Knapp (Ref. 22) measured the exchange splittings and the d-band widths of transition metals. They found for Fe an exchange splitting of 1.5 eV at the P_4 point (s-d hybridized). To obtain the same exchange splitting at this point we need an exchange coupling constant J for the pure d bands of 1.78 eV.

[22] D. E. Eastman, F. J. Himpsel, and J. A. Knapp, Phys. Rev. Lett. **44**, 95 (1980).

[23] P. N. Argyres, Phys. Rev. **97**, 334 (1955).

[24] J. Callaway and C. S. Wang, Phys. Rev. B **16**, 2095 (1977).

[25] K. B. Hathaway, H. J. F. Jansen, and A. J. Freeman, Phys. Rev. B **31**, 7603 (1985).

[26] Note, iron lacks the strong effects due to many-body excitations very close to the Fermi level present in nickel and which give an additional sign change in the experimental MOKE spectrum of nickel for frequencies below 0.5 eV (Refs. 9 and 11).

[27] Although the experiment of Krinchik (Ref. 9) covers a large range of frequency, the position of the first peak seems to be at too low frequencies. However, regarding the ratio of peak heights we find good agreement with the experiment by Krinchik.

[28] P. M. Oppeneer, J. Sticht, T. Maurer, and J. Kübler, Z. Phys. B **88**, 309 (1992).

[29] W. Hübner and K. H. Bennemann, Vacuum **41**, 514 (1990).

[30] A more careful consideration should include the ω dependence. Obviously, for determining $\left(\frac{\chi^{(2)}_{\mathrm{mag}}}{\chi^{(2)}_{\mathrm{nonmag}}}\right)_{\mathrm{Fe}}$ exactly, one must calculate $\chi^{(2)}_{zzz}$ for Fe (Ref. 31) and include the detailed geometry of the experiment as well as the ellipticities of (i) the nonlinear Kerr effect, (ii) second-harmonic generation, and (iii) the polarizer in the reflected frequency-doubled beam.

[31] Note, $\chi^{(2)}_{zzz}$ is also needed for calculating the Kerr angle referring to the polarization of the second harmonic: $\Phi_K(\mathrm{SHG}) \approx \chi^{(2)}_{xzz}/\chi^{(2)}_{zzz}$. Regarding $\Phi_K(\mathrm{SHG})$, we expect from our theory particularly interesting results if large $\lambda_{\mathrm{s.o.}}$ and magnetic moments are present. For example, this may be the case for Heusler alloys.

[32] G. L. Richmond, J. M. Robinson, and V. L. Shannon, Prog. Surf. Sci. **28**, 1 (1988).

[33] Reif *et al.* also point out that in agreement with our theory the nonlinear Kerr effect may be observed at coated magnetic surfaces and at film interfaces and is not restricted to remanence magnetization measurement.

[34] N. V. Cohan and H. F. Hameka, Physica **37**, 320 (1967).

[35] C. Kittel, Phys. Rev. **83**, 208(A) (1951).